ACS Catalysis

Research Article

pubs.acs.org/acscatalysis

Pt@Nb-TiO_2 Catalyst Membranes Fabricated by Electrospinning and Atomic Layer Deposition

Qing Du

Department of Chemical Engineering, University of Rochester, Rochester, New York 14627, United States

Jianbo Wu and Hong Yang*

Department of Chemical and Biomolecular Engineering, University of Illinois at Urbana−Champaign, 114 Roger Adams Laboratory, MC-712, 600 S. Mathews Avenue, Urbana, Illinois 61801, United States

Supporting Information

ABSTRACT: A facile method was developed to fabricate fibrous membranes of niobium-doped titania-supported platinum catalysts (Pt@Nb-TiO_2) by a two-step approach. The process started with generating niobium-doped titania (Nb-TiO_2) fibrous membranes by electrospinning, followed by the deposition of Pt nanoparticles (NPs) using an atomic layer deposition (ALD) technique. The area-specific oxygen reduction reaction (ORR) activity of Pt@TiO_2 catalyst membrane was increased by ∼20 folds if 10 at.% of Nb was incorporated into the ceramic fibers. The area-specific activity also increased with the number of ALD cycles, because of the increase of the Pt loading in the catalysts. After post-treatment of the catalyst membrane at high temperature in H_2-containing atmosphere, the ORR activity became 0.28 mA/cm^2_{Pt} at 0.9 V (vs RHE), because of the improvement in conductivity of Nb-TiO_2 fibers and better crystalinity of Pt NPs. The results of accelerated-stability test showed that the Pt@Nb-TiO_2 catalyst membrane was highly stable and lost only 10% of its initial activity after 30 000 potential cycles (0.6 to 1.0 V vs RHE) under a strong acidic condition.

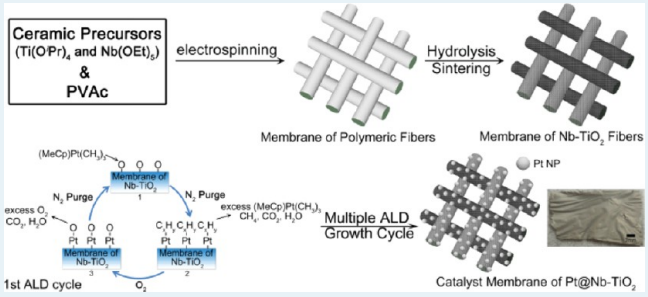

KEYWORDS: *electrospinning, atomic layer deposition, ALD, Pt nanoparticle, titania, membrane, ORR*

1. INTRODUCTION

Polymer electrolyte membrane fuel cells (PEMFCs) are important for the development of green technology in energy storage and conversion.[1] In a PEMFC, supported Pt and Pt alloys are the main electrocatalysts for the oxygen-reduction reaction (ORR).[2] Besides electrocatalysts, support is also critically important. Carbon black has been used as the supporting material for catalysts, because of its large surface area, high electrical conductivity, and well-developed pore structure.[3] However, carbon tends to be corroded under the harsh electrochemical reaction conditions.[4] Corrosion of the carbon support causes the agglomeration and sintering of Pt catalyst particles, resulting in decreases of electrochemical surface area (ECSA) and activity of the catalysts. Carbon corrosion also leads to isolated Pt particles detaching from the support. In addition, it has been found that Pt catalysts accelerate the corrosion rate of the carbon support.[5] These effects strongly affect the durability of PEMFCs; therefore, noncarbon supports increasingly attract a great deal of attention.[6]

Titanium dioxide (TiO_2) has been considered as an alternative for the support material, because it has excellent stability in both acidic and oxidative environments.[7] To use TiO_2 as an electrocatalyst support, one need develop a new approach to the deposition of highly active catalysts on TiO_2. The support must be conductive, because the conductivity of TiO_2 is several orders of magnitude lower than that of carbon black (Vulcan XC-72). In this context, electrospinning and atomic layer deposition (ALD) are both simple and controllable techniques. The combination of these two is likely suitable for production of TiO_2-supported Pt catalysts. Membranes that consisted of one-dimensional TiO_2 fibers with high surface area were made before by electrospinning.[6a,8] The ALD technique is capable of depositing uniform NPs without capping ligands on granular and porous materials, thus avoiding surface contaminations by organic capping molecules. In addition, a high degree of control over the size of NPs is possible, using the ALD technique, because of its ability to precisely control the delivery of chemical reagents and the self-limiting nature of the surface-saturated reactions mechanism.[9] Compared with currently available Pt/C catalysts, Pt NPs are anchored on the surface of supports through ALD instead of simple mixing.

Received: October 17, 2013
Revised: December 1, 2013
Published: December 2, 2013

This chemical process helps anchor NPs on the ceramic fiber surfaces, thus potentially increasing the stability of the catalysts.

A typical method for improving the conductivity of TiO_2 is through incorporation of *n*-type dopants, such as vanadium-(V),[10] niobium (Nb),[6d,11] and tantalum (Ta).[12] Another approach is heat treatment at high temperatures under reducing atmosphere in order to create oxygen vacancies in TiO_2.[13] When the dopant method is used, Nb is often preferred; since Nb^{5+} (r = 0.70 Å) has similar ionic radius as Ti^{4+} (r = 0.68 Å), there exists negligible lattice mismatch between TiO_2 and Nb_2O_5. Thus, Nb_2O_5 forms a complete range of solid solutions with TiO_2.[11,14]

In this work, we present an innovative approach for making catalyst membranes of Pt NPs on Nb-doped TiO_2 fiber membranes. This approach is developed based on the recent success in two independent areas, namely, the fabrication of TiO_2 fibers by electrospinning[8] and the deposition of Pt NPs on supports, such as WC,[9b] Al_2O_3,[15] $SrTiO_3$[9c,16] and carbon nanotube by ALD.[17] These catalyst membranes could potentially be directly integrated in membrane electrode assembly (MEA) as the catalyst layer, avoiding complicated process of making catalyst inks and then spraying or painting them onto a gas diffusion layer, because the catalyst layer is already in a membrane form. The effects of Nb amount, conditions for ALD, and post-treatment on electrocatalytic activity and stability of the membranes are studied.

2. EXPERIMENTAL SECTION

2.1. Materials. Polyvinyl acetate (PVAc, M_w 500 000), titanium(IV) isopropoxide ($Ti(O^iPr)_4$, 99.999%), and niobium ethoxide ($Nb(OEt)_5$, 99.95%) were purchased from Sigma–Aldrich. *N*,*N*-dimethyl formamide (DMF, anhydrous) was obtained from Honeywell Burdick and Jackson. Acetic acid (glacial, 99.7%) was from Alfa Aesar. Nafion 117 solution was from Fluka. All chemicals were used as received without further purification.

2.2. Synthesis of Membrane Supports Made of Nb-TiO_2 Fibers. Typically, 0.123 g of PVAc was dissolved in 1 mL of DMF in a glovebox.[11] After complete dissolution, $Ti(O^iPr)_4$, $Nb(OEt)_5$, and 0.119 g of acetic acid were added into the solution in a glovebox. The atomic ratio of $Ti(O^iPr)_4$ and $Nb(OEt)_5$ was varied according to the predetermined Nb percentage, while the total amount of Ti and Nb was kept at 1.67 mmol. The resulting solution was mixed well and electrospun at an accelerating voltage of 20 kV and at a flow rate of 1 mL/h. The membrane of polymeric fibers was collected on a grounded aluminum foil placed 15 cm below the spinneret. The relative humidity (RH) of the environment was kept above 40%. The formed membrane was peeled off from foil using tweezers and left in the air for ∼10 h. The membrane was then pyrolyzed in air at 500 °C for 24 h to remove PVAc and generate Nb-TiO_2 fibers.

2.3. Synthesis of Membranes of Pt@Nb-TiO_2 Catalysts. ALD is utilized to deposit Pt NPs onto the membrane of Nb-TiO_2 supports. The membrane of Nb-TiO_2 fibers was fixed in a chuck and hung in the air inside the chamber of an ALD system (Savannah 100 and 200, Cambridge Nano Tech, Inc.) to ensure that both sides of the membrane are exposed to the reactants. The chamber was kept at 270 °C. A platinum precursor, trimethyl(methylcyclopentadienyl) platinum(IV) ((MeCp)Pt-$(CH_3)_3$), was kept at 70 °C and gas lines were held at 150 °C to avoid any condensation of precursors. High-purity O_2 was used as the coreactant in the ALD process. High-purity N_2 was used as both the carrier and the purge gas. The flow rate of N_2 gas was maintained at 5 sccm. A typical ALD cycle was as follows: 2 s of Pt precursor pulse, 5 s of N_2 purge, 2 s of O_2 pulse, and 28 s of N_2 purge. Pt NPs with different sizes were obtained by changing the total number of ALD growth cycle. For electrochemical measurement, catalyst membrane of Pt@Nb-TiO_2 was treated at either 200 or 500 °C in 5% H_2 in an argon atmosphere for 2 h.

2.4. Electrochemical Measurement. A three-electrode cell was used to perform the electrochemical measurements. The working electrode was a glassy-carbon rotating-disk electrode (RDE; area = 0.196 cm^2). Pt foil (1 cm × 1 cm) was used as the counter electrode. A reversible hydrogen electrode (RHE) was used as the reference electrode, which was placed in a separate compartment. The electrolyte for all of the measurements was 0.1 M perchloric acid, which was diluted with deionized water from a 70% doubly distilled stock solution (GFS Chemicals, USA). To prepare the working electrode, the Pt@Nb-TiO_2 catalyst was first dispersed in ethanol and the mixture was sonicated for 30 min. Five microliters (5 μL) of suspension was added onto RDE by a pipet and dried under air. It was repeated until the surface of RDE was covered by a thin uniform layer of the catalysts. The loading amount was 0.6 mg_{Pt}/cm^2. Then, 10 μL of 0.0125% (w/w) Nafion-ethanol solution was dropped on the surface of the thin film to prevent the catalysts from detaching by the flow of testing solution. The measurements of the total electrochemically active surface area (ECSA) were performed by integrating the hydrogen adsorption from the cyclic voltammetry (CV) data, which was recorded at room temperature in an argon-saturated solution of 0.1 M $HClO_4$. The potential scan rate was 50 mV s^{-1} for the CV measurements. The ORR measurements were conducted at a rotation rate of 1600 rpm in 0.1 M $HClO_4$, which was purged with oxygen for 30 min prior to and during the measurements. The scan rate for the ORR measurement was 10 mV s^{-1} in the positive direction. The accelerated-stability test (ADT) was conducted at ambient temperature in an Ar-protected 0.1 M solution of aqueous $HClO_4$. Before the ADT, samples were pretreated by running 40 CV cycles between 0.05 and 1.0 V (versus RHE) to active the catalysts. The potential was cycled 30 000 times between 0.6 and 1.0 V (versus RHE) at a scan rate of 100 mV s^{-1}, and the polarization curves were recorded after every 10 000 cycles. The area-specific activity was obtained by normalizing the kinetic current density against the ECSA values, and the kinetic current density was obtained from the Koutecky–Levich plot.

2.5. Characterization. The morphology of the fibers and Pt@Nb-TiO_2 catalyst membrane were studied by field-emission scanning electron microscopy (FE-SEM) (Zeiss-Leo, Model DSM982) and field-emission transmission electron microscopy (FE-TEM) (FEI TECNAI, Model F-20). Average diameter of fibers and Pt nanoparticles were measured and calculated using Image J (National Institutes of Health (NIH), USA). The average sizes were based on more than 150 NPs on three or more SEM images. The Pt NPs were spherical when the total number of ALD cycles was <40. As the number of ALD cycles increased, the size of Pt NPs grew and the distance between isolated Pt NPs decreased until the Pt nanocrystals came into connect with each other. Under this circumstance, the average diameters of primary particles were measured; otherwise, the length of the Pt NPs were measured and used. Scanning transmission electron microscopy (STEM) and elemental maps were carried out using the high-angle annular dark field

dx.doi.org/10.1021/cs400944p | ACS Catal. 2014, 4, 144–151

Scheme 1. Schematic Illustration of the Process for the Production of Pt@Nb-TiO_2 Catalyst Membrane: (A) Preparation of Nb-TiO_2 Fiber-Woven Membrane by Electrospinning Technique and through Pyrolysis and (B) Deposition of Pt NPs onto a Nb-TiO_2 Fiber Membrane by the ALD Technique[a]

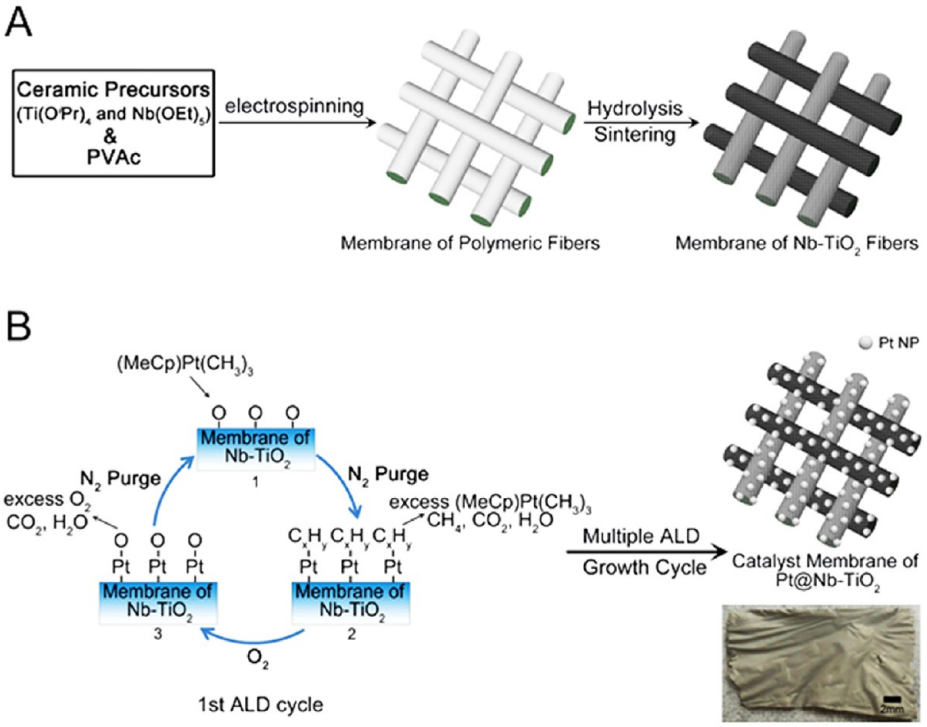

[a]The photograph shows a final membrane made of Pt@Nb-TiO_2 fibers.

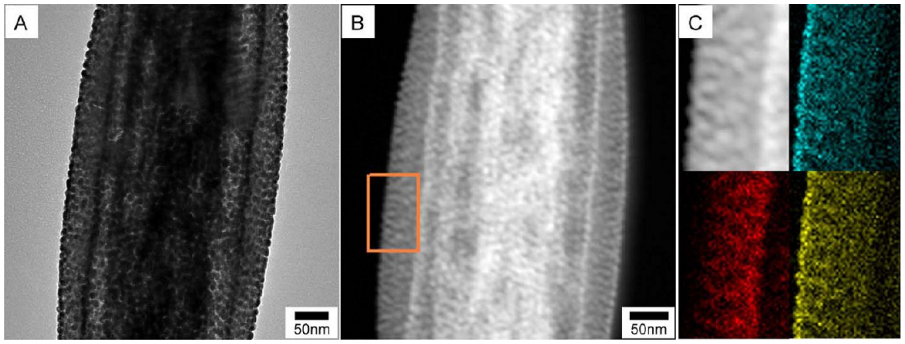

Figure 1. (A) TEM and (B) STEM micrographs of Pt@Nb-TiO_2 catalyst. (C) HAADF-STEM study showing the distribution of Pt (blue), Ti (red), and Nb (green) elements. The area for HAADF-STEM study is the marked region in panel (B).

(HAADF) mode on the FE-TEM system. Energy-dispersive X-ray (EDX) analysis was carried out on an FE-SEMsystem that was equipped with an energy-dispersive X-ray analysis spectroscopy (EDAX) detector. Powder X-ray diffraction (PXRD) patterns were recorded on a Philips MPD diffractometer with a Cu K_α X-ray source (λ = 1.5405 Å).

3. RESULTS AND DISCUSSION

3.1. Synthesis of the Pt@Nb-TiO_2 Catalyst Membranes. Scheme 1 illustrates the two-step process for the fabrication of catalyst membrane by combining the electrospinning and ALD techniques. First, a membrane of Nb-TiO_2 fibers was made from sol–gel precursors by electrospinning and after the polycondensation (Scheme 1A). The process began with the generation of polymeric fibers from a mixture of ceramic precursors ($Ti(O^iPr)_4$ and $Nb(OEt)_5$) and guiding polymer PVAc by electrospinning. The Nb amount was controlled by adding the proper amount of $Nb(OEt)_5$, based on the predetermined atomic ratio between $Ti(O^iPr)_4$ and $Nb(OEt)_5$. The Nb-TiO_2 fiber membranes were obtained through hydrolysis and condensation in air. Second, the ALD technique was used to deposit Pt NPs onto the membranes whose thickness was between 5 and 10 μm. Typically, an ALD cycle began with a organometallic precursor ((MeCp)Pt-$(CH_3)_3$) pulse. $(MeCp)Pt(CH_3)_3$ reacted with O atoms on the surface of Nb-TiO_2 membranes, generating PtC_xH_y-containing compounds and byproducts of CH_4, CO_2 and H_2O. The excess $(MeCp)Pt(CH_3)_3$ and byproducts were cleared by N_2 purging gas, followed by the O_2 pulse. O_2 reacted with the PtC_xH_y segment to form Pt–O and byproduct, CO_2 and H_2O. The O atom generated could be used to react with $(MeCp)Pt(CH_3)_3$ in the subsequent ALD cycle. The ALD cycle was finished by another N_2 purge to eliminate excess O_2 and byproducts. By repeating the ALD growth cycle, different size of Pt NPs could

dx.doi.org/10.1021/cs400944p | ACS Catal. 2014, 4, 144–151

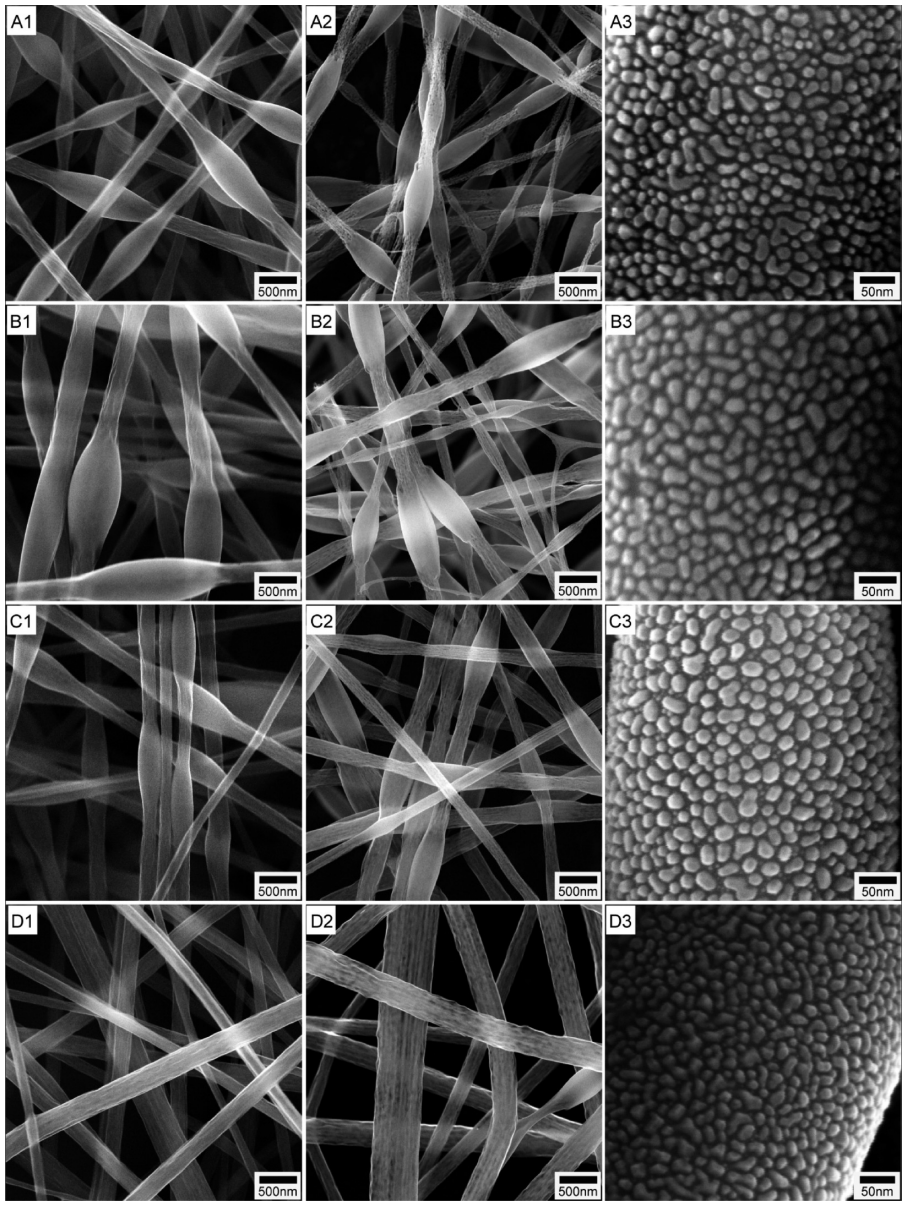

Figure 2. SEM images of (A1, B1, C1, and D1) as-spun polymeric fibers, (A2, B2, C2, and D2) Nb-TiO_2 fibers after hydrolysis and sintering, and (A3, B3, C3 and D3) Pt@Nb-TiO_2 catalysts after a 40-cycle ALD of Pt NPs. The amount of Nb was (A) 0 at.%, (B) 5 at.%, (C) 10 at.%, and (D) 25 at.%, separately.

be deposited onto the Nb-TiO_2 membrane, because the reaction streams of $(MeCp)Pt(CH_3)_3$ and O_2 were separated by a purge gas of N_2. During each reactant pulse, only one reactant reacted with the substrate surface, through a self-limiting process that was capable of precisely controlling the growth of Pt NPs.

Figure 1 shows the TEM, STEM, and HAADF-STEM micrographs of Pt NPs dispersed on a Nb-TiO_2 fiber made after 40 ALD cycles. The patchy, uneven contrast shown in the TEM micrograph indicates that the surface of Nb-TiO_2 fiber was not smooth. Both TEM and STEM micrographs show that the Pt NPs were uniformly dispersed on the ceramic fibers with an average diameter of 14 nm. Several studies previously show the dispersion of Pt particles increased as the number of oxygen-containing surface species in the support increased.[18] In this system, Nb-TiO_2 fibers contained abundant oxygen surface groups. As a result, the deposition of Pt NPs was uniform. The HAADF-STEM micrograph indicates that elemental Pt, Ti, and Nb were distributed homogeneously throughout the Nb-TiO_2 fiber. These results indicate metal nanoparticles with high uniformity in size could be deposited onto metal oxide fiber membranes by electrospinning and ALD techniques. This two-step process is easy to operate and scalable, because the size of the membrane generated by electrospinning and ALD could be very large, depending on the scale of the equipment. In our experiment, the size of a typical membrane was 1.5 cm × 2.2 cm (see insert in Scheme 1B).

3.2. Composition and Electrocatalytic Activity Relationship of Pt@Nb-TiO_2 Membranes. Nb-TiO_2 support membranes with 5, 10, and 25 at.% of Nb were prepared by varying the $Nb(OEt)_5/Ti(O^iPr)_4$ atomic ratio from 5:95, to 10:90, and to 25:75 in the electrospun solution. Pt NPs were loaded onto these membranes by 40 ALD cycles. Figure 2 shows SEM images of as-spun polymeric fibers (left column),

dx.doi.org/10.1021/cs400944p | ACS Catal. 2014, 4, 144−151

Nb-TiO_2 fibers (middle column), and Pt@Nb-TiO_2 catalysts (right column). Table 1 summarizes the diameter of the fibers

Table 1. Diameters of the Fibers and Size of Beads of As-Spun Polymeric and Nb-TiO_2 Ceramic Fibers at Different Amounts of Nb (at%)

	As-Spun Polymeric Fiber		Nb-TiO_2 Fiber	
amount of Nb (at.%)	fiber (nm)	bead (nm)	fiber (nm)	bead (nm)
0	193	405	152	321
5	212	426	157	356
10	183	368	170	343
25	270		220	

and size of the beads of as-spun polymeric and ceramic Nb-TiO_2 fibers with different doping amounts of Nb. The diameter of Nb-TiO_2 fibers did not change much, when compared with the as-spun polymeric fibers. Void spaces were generated after the pyrolysis in air due to the removal of PVAc and to the homogeneous nature of the preceramic mixture of PVAc and metal alkoxide precursors (Figure 2, middle column images). The ceramic fibers were continuous and made of small, crystal domains without preferred orientation (Figure 3). Although the

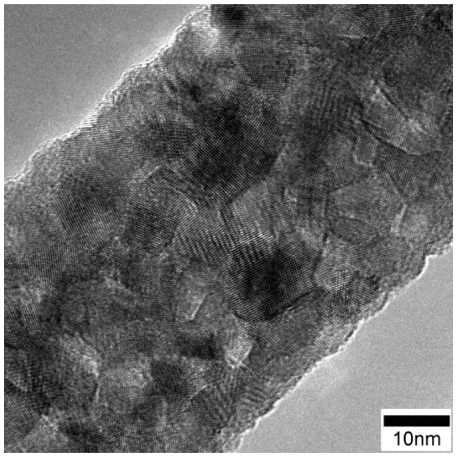

Figure 3. TEM micrograph of TiO_2 fiber.

morphologies of fibers were different at the different compositions of the Nb-TiO_2 ceramic, the average diameters of Pt NPs were ~14 nm for all three samples, based on the analysis of more than 150 NPs from multiple SEM images. Thus, the size of Pt NPs apparently depended only on the operating temperatures of the Pt precursors and ALD chamber, and the number of ALD cycles.[19]

XRD patterns of Nb-TiO_2 support membranes show the diffraction peaks, which could be assigned to anatase phase of TiO_2 (Figure 4). No diffraction peaks from niobium oxide were observed, which indicates that Nb was incorporated into the TiO_2 crystal structure. The formation of mixed oxide ceramic could be attributed to the similar ionic radii between the two metal ions. Increased Nb amount in the ceramic resulted in large lattice strain and a shift in the lattice parameters.[20] The XRD peaks of Nb-TiO_2 shifted to the low 2θ angles gradually when the amount of Nb increased, primarily because of the relative large radius of Nb.

Figure 5 shows the dependence of area-specific ORR activities (i_s) of Pt@Nb-TiO_2 catalyst membranes on the amount of Nb. The ORR polarization curves of the four

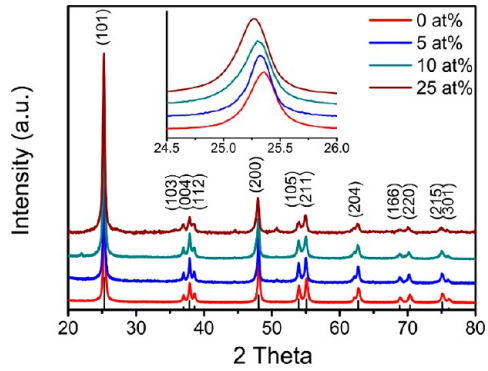

Figure 4. XRD patterns of Nb-TiO_2 fibers with different amount of Nb. XRD patterns of anatase TiO_2 are shown by the black lines as a reference based on the JCPDS database (No. 84-1286).

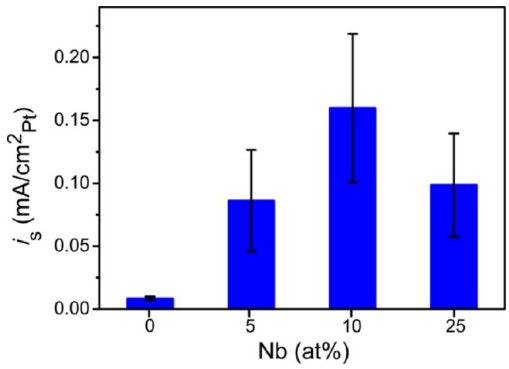

Figure 5. Dependence of area-specific ORR activities of Pt@Nb-TiO_2 catalyst membrane at 0.9 V (versus RHE) on Nb-doped percentage in the fiber ceramics.

samples were shown in Figure S1 in the Supporting Information. The area-specific activity changed from 0.0084 mA/cm$^2_{Pt}$ for Pt@TiO_2, to 0.086 mA/cm$^2_{Pt}$ for Pt@Nb-TiO_2 with 5 at.% Nb, and to 0.16 mA/cm$^2_{Pt}$ for Pt@Nb-TiO_2 with 10 at.% Nb at 0.9 V (versus RHE). The catalyst membrane of Pt@Nb-TiO_2 with 10 at.% Nb showed an ~20-fold enhancement in ORR activity over the Pt@TiO_2 membrane. Increasing the Nb amount further to 25% did not result in a further increase in ORR activity. Since there was no major difference in size and shape of the Pt NPs, the change in catalytic activity could largely attributed to the Nb-TiO_2 fiber membranes. It is known that the conductivity of Nb-doped TiO_2 increases with the relative amount of Nb in thin films[21] and powders.[22] Wang et al. reported that the conductivity of Nb-doped titania powders changed from 4.9×10^{-8} S cm^{-1}, to 9.6×10^{-7} S cm^{-1}, to 7.9×10^{-5} S cm^{-1}, and to 1.2×10^{-3} S cm^{-1} when the amount of Nb increased from 0 at.%, to 5 at.%, to 10 at.%, and to 20 at.%.[22b] Thus, the area-specific ORR activities of Pt@Nb-TiO_2 catalyst membrane increased because of the improvement of conductivity of the ceramic supports. While the activity for Pt@Nb-TiO_2 fiber membrane appeared to be different, the values were still within the measurement errors, although the morphology of the fibers (with or without beads) might cause the difference in the deposition of Pt NPs.

3.3. Effect of ALD Cycles and Post-Treatment on Electrocatalytic Activity. ALD is typically used to deposit thin films of oxides on flat substrate through a self-limiting process. When ALD was used to grow Pt on substrates, however, discrete Pt NPs formed and dispersed uniformly over

dx.doi.org/10.1021/cs400944p | ACS Catal. 2014, 4, 144−151

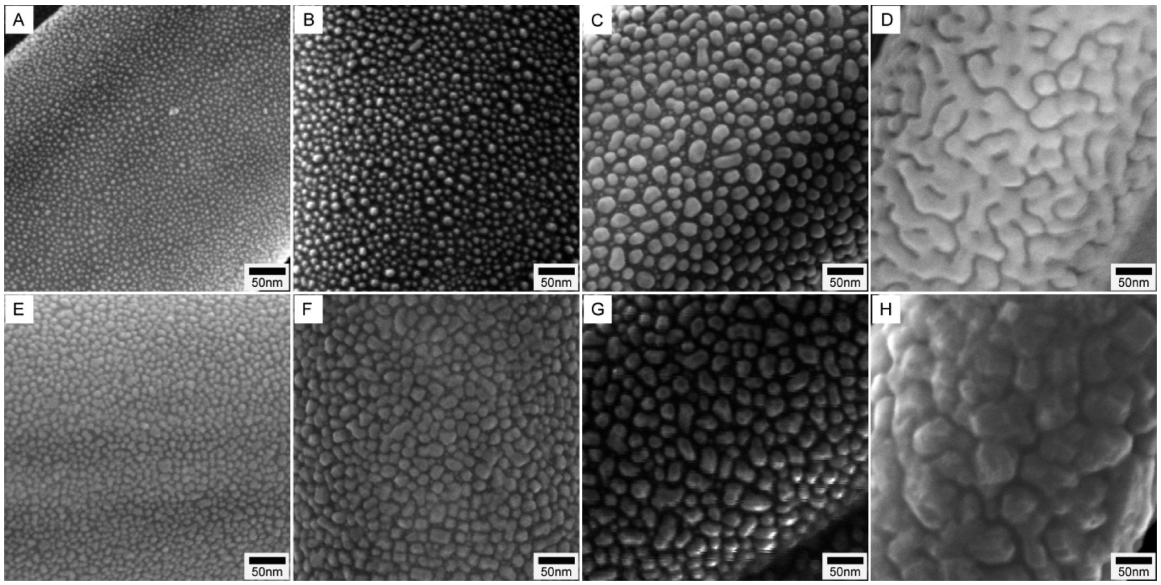

Figure 6. SEM images of Pt@Nb-TiO_2 catalysts with 10 at.% Nb after post-treatment in 5% H_2 in argon at (A–D) 200 °C and (E–H) 500 °C, respectively. The numbers of ALD cycle were as follows: (A, E) 10, (B, F) 20, (C, G) 40, and (D, H) 80.

the supports (Figure 6). As the number of ALD cycles increased, the size of Pt NPs grew and the distance between isolated Pt NPs decreased (see Figures 6A and 6C) until the Pt nanocrystals came into contact with each other (Figure 6D). Normally, the difference in reactivity between the substrate and the Pt active sites led to a preference for Pt NPs to grow by itself, rather than to nucleate new particles on the substrate. But sometimes, new particles also nucleated with the growth of large Pt NPs, showing obvious small particles (Figure 6C). The average sizes of Pt NPs on Nb-TiO_2 with 10 at.% of Nb were 4.5 nm after the growth of 10 ALD cycles, 9.2 nm after 20 cycles, and 14 nm for 40 cycles at the post-treatment temperature of 200 °C. If the number of ALD cycles increased to 80, the Pt particles came into connect with each other.

As the ALD process of Pt ended with an oxygen pulse, the outer layer of Pt NPs was covered with PtO (see Scheme 1B).[19b] Thus, the catalyst membranes of Pt@Nb-TiO_2 were post-treated at 200 °C in 5% H_2 in argon to reduce PtO to Pt. This procedure did not affect the size and morphology of Pt NPs. To check the effect of temperature on ORR activity, the membranes were treated at 500 °C in 5% H_2 in Ar. At this temperature, the size and morphology of Pt NPs changed, because Pt atoms migrated and coalesced on the surface of support, according to the Smoluchowski model. Atoms from small Pt NPs could move and grow on large ones through the Ostwald ripening process, resulting in further growth of Pt NPs when post-treated at 500 °C.[23] The sizes of Pt NPs increased to 7.5 nm for samples made after 10 ALD cycles, 12.6 nm after 20 cycles, and 18.7 nm after 40 cycles. The Pt particles also became connected if the number of ALD cycle increased to 80 (Figure 6H). In addition, the surface of Pt NPs became faceted (see Figures 6G and 6H).

The area-specific ORR activities of catalyst membranes of Pt@Nb-TiO_2 with 10 at.% Nb increased with the number of ALD cycles (see Figure 7). The weight percentage of Pt in the catalyst increased from 49% for a catalyst membrane with 10 ALD cycles, to 65% with 20 cycles, to 80% with 40 cycles, and to 87% with 80 cycles, based on the energy-dispersive X-ray (EDX) analysis. The increase in weight percentage of Pt NPs could also help to improve the conductivity of the catalyst membrane.

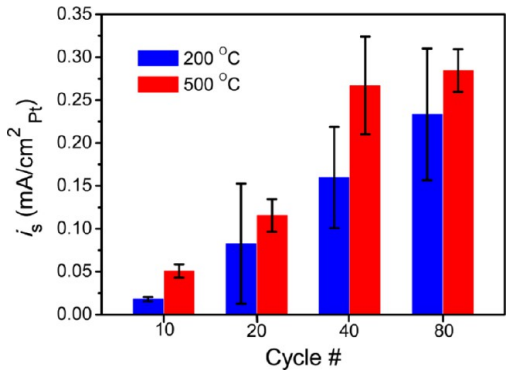

Figure 7. Dependence of area-specific ORR activities of Pt@Nb-TiO_2 with 10 at.% Nb at 0.9 V (versus RHE) on the number of ALD cycles for making Pt NPs, and the temperature of post-treatment in 5% H_2 in argon.

Comparing area-specific activities of the Pt@Nb-TiO_2 catalyst membranes with the Pt NPs deposited by the same number of ALD cycles, the one that was post-treated at 500 °C had higher activities. One reason was the increase of crystallinity of Pt NPs, which was improved after the post-treatment at high temperature. In addition, hydrogen treatment at high temperature could result in hydrogen doping into the Nb-TiO_2 support.[13] The *n*-type TiO_2 formed by introducing hydrogen interstitial or substitution sites.[24] Thus, the conductivity of the support was further increased. As a result, the area-specific activity of catalyst membrane treated at 500 °C in H_2 atmosphere was higher than those treated at 200 °C.

3.4. Accelerated-Stability Test. Accelerated-stability test was conducted to examine the electrochemical stability of the Pt@Nb-TiO_2 catalyst with 10 at.% Nb. The sample was pretreated by 40 cycles of cyclic voltammetry (CV) measurement between 0.05 V and 1.0 V (versus RHE) before the test to active the catalyst. For the stability test, the potential was cycled 30 000 times between 0.6 V and 1.0 V (versus RHE), while the

dx.doi.org/10.1021/cs400944p | *ACS Catal.* 2014, 4, 144–151

ORR and CV measurements were performed every 10 000 cycles (Figure 8). Table 2 summarizes the electrochemically active surface area (ECSA), kinetic-current density (i_k), and area-specific activity (i_s) at 0.9 V (versus RHE). The ORR polarization curves barely changed after the 30 000th-cycle accelerated stability test, indicating that the catalyst membranes were very stable. Kinetic current density decreased only slightly and within 10% of its original value after the test, although area-specific activity decreased 25%. The total ECSA increased slightly after the stability study. This result is uncommon, because the ECSA value of the catalysts typically decreased after the accelerated-stability test, because of corrosion of the catalyst support, agglomeration and sintering of Pt particles, and the detachment of Pt particles from the supports.[4a,b,d] TEM micrographs of Pt@Nb-TiO_2 catalyst with 10 at.% Nb before and after the 30 000th-cycle accelerated-stability test shows that the catalysts were kept largely intact and the size of the Pt NPs did not experience an obvious change (Figure 9). Thus, the increase is attributed largely to the further exposure of active Pt sites, which were not accessible before the cycles, and possibly to the removal of surface impurity.

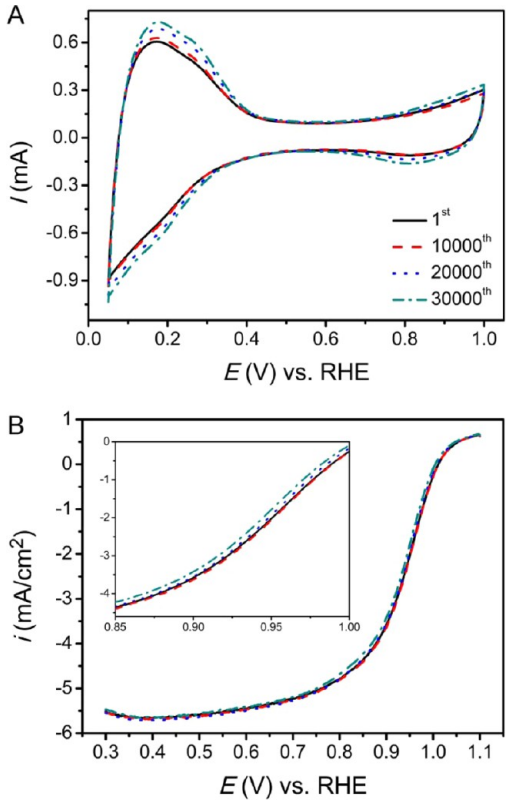

Figure 8. Accelerated-stability test of Pt@Nb-TiO_2 catalyst with 10 at.% Nb: (A) CV curves and (B) ORR polarization curves measured at 1600 rpm.

Table 2. Electrochemically Active Surface Area (ECSA), Kinetic Current Density (i_k), and Area-Specific Current Density (I_s) at 0.9 V (versus RHE) of Pt@Nb-TiO_2 Catalyst Membranes with 10 at.% Nb after a Given Number of Potential Cycles during the Accelerated-Stability Test[a]

cycle number	ECSA (cm^2)	i_k (mA/cm^2)	i_s (mA/cm^2_{Pt})
1st	14.74	15.87 (100%)	0.21 (100%)
10 000th	15.80	16.25 (102%)	0.20 (96%)
20 000th	16.61	15.13 (95%)	0.18 (85%)
30 000th	17.44	14.15 (89%)	0.16 (75%)

[a]Relative percentages are given in parentheses.

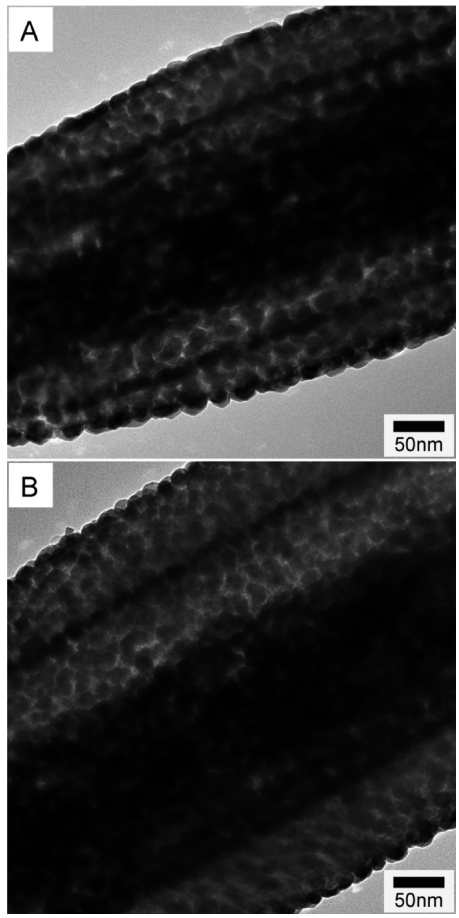

Figure 9. TEM micrographs of Pt@Nb-TiO_2 catalyst with 10 at.% Nb (A) before and (B) after the accelerated-stability test.

4. CONCLUSIONS

A method that combines the electrospinning and atomic layer deposition (ALD) techniques was developed to fabricate Pt@Nb-TiO_2 catalyst membranes. The conductivity of the membrane increased with the amount of Nb incorporated in the TiO_2 ceramic fibers. The area-specific oxygen reduction reaction (ORR) activities of the catalysts increased from 0.0084 mA/cm^2_{Pt} for Pt@TiO_2 to 0.28 mA/cm^2_{Pt} for Pt@Nb-TiO_2 with 10 at.% Nb at 0.9 V (versus RHE) after post-treatment at 500 °C. The accelerated-stability test on the Pt@Nb-TiO_2 catalyst membrane showed that it has very high stability with only an ~10% loss in ORR activity. This preparation method is good for making uniform catalysts on various types of oxide supports with tunable conductivity and without the need for surface organic ligand in a controllable fashion.

■ ASSOCIATED CONTENT

Supporting Information

This material is available free of charge via the Internet at http://pubs.acs.org.

dx.doi.org/10.1021/cs400944p | ACS Catal. 2014, 4, 144−151

AUTHOR INFORMATION

Corresponding Author

*E-mail: hy66@illinois.edu.

Notes

The authors declare no competing financial interest.

ACKNOWLEDGMENTS

This work was supported in part by the Laboratory for Laser Energetics, NSF (Grant No.: CHE-1213926) and a start-up fund from the University of Illinois.

REFERENCES

(1) (a) Baxter, J.; Bian, Z. X.; Chen, G.; Danielson, D.; Dresselhaus, M. S.; Fedorov, A. G.; Fisher, T. S.; Jones, C. W.; Maginn, E.; Kortshagen, U.; Manthiram, A.; Nozik, A.; Rolison, D. R.; Sands, T.; Shi, L.; Sholl, D.; Wu, Y. Y. *Energy Environ. Sci.* **2009**, *2*, 559−588. (b) Carrette, L.; Friedrich, K. A.; Stimming, U. *ChemPhysChem* **2000**, *1*, 162−193. (c) Ogden, J. M. *Annu. Rev. Energy Environ.* **1999**, *24*, 227−279. (d) Sopian, K.; Daud, W. R. W. *Renew. Energy* **2006**, *31*, 719−727. (e) Wagner, F. T.; Lakshmanan, B.; Mathias, M. F. *J. Phys. Chem. Lett.* **2010**, *1*, 2204−2219.

(2) (a) Debe, M. K. *Nature* **2012**, *486*, 43−51. (b) Peng, Z. M.; Yang, H. *Nano Today* **2009**, *4*, 143−164. (c) Xia, Y. N.; Xiong, Y. J.; Lim, B.; Skrabalak, S. E. *Angew. Chem., Int. Edit.* **2009**, *48*, 60−103. (d) Wu, J.; Yang, H. *Acc. Chem. Res.* **2013**, *46*, 1848−1857.

(3) Dicks, A. L. *J. Power Sources* **2006**, *156*, 128−141.

(4) (a) Hasche, F.; Oezaslan, M.; Strasser, P. *Phys. Chem. Chem. Phys.* **2010**, *12*, 15251−15258. (b) Koh, S.; Leisch, J.; Toney, M. F.; Strasser, P. *J. Phys. Chem. C* **2007**, *111*, 3744−3752. (c) Li, W.; Lane, A. M. *Electrochem. Commun.* **2009**, *11*, 1187−1190. (d) von Deak, D.; Biddinger, E. J.; Ozkan, U. S. *J. Appl. Electrochem.* **2011**, *41*, 757−763.

(5) (a) Ferreira, P. J.; la O', G. J.; Shao-Horn, Y.; Morgan, D.; Makharia, R.; Kocha, S.; Gasteiger, H. A. *J. Electrochem. Soc.* **2005**, *152*, A2256−A2271. (b) Shao, Y. Y.; Yin, G. P.; Gao, Y. Z. *J. Power Sources* **2007**, *171*, 558−566.

(6) (a) Formo, E.; Lee, E.; Campbell, D.; Xia, Y. N. *Nano Lett.* **2008**, *8*, 668−672. (b) Gojkovic, S. L.; Babic, B. M.; Radmilovic, V. R.; Krstajic, N. V. *J. Electroanal. Chem.* **2010**, *639*, 161−166. (c) Huang, S. Y.; Ganesan, P.; Park, S.; Popov, B. N. *J. Am. Chem. Soc.* **2009**, *131*, 13898−13899. (d) Huang, S. Y.; Ganesan, P.; Popov, B. N. *Appl. Catal., B* **2010**, *96*, 224−231. (e) Lim, D. H.; Lee, W. J.; Macy, N. L.; Smyrl, W. H. *Electrochem. Solid State Lett.* **2009**, *12*, B123−B125. (f) Park, K. W.; Seol, K. S. *Electrochem. Commun.* **2007**, *9*, 2256−2260. (g) von Kraemer, S.; Wikander, J.; Lindbergh, G.; Lundblad, A.; Palmqvist, A. E. C. *J. Power Sources* **2008**, *180*, 185−190. (h) Cavaliere, S.; Subianto, S.; Savych, I.; Jones, D. J.; Roziere, J. *Energy Environ. Sci.* **2011**, *4*, 4761−4785.

(7) Liu, Z. M.; Zhang, J. L.; Han, B. X.; Du, J. M.; Mu, T. C.; Wang, Y.; Sun, Z. Y. *Microporous Mesoporous Mater.* **2005**, *81*, 169−174.

(8) (a) Ding, B.; Kim, H.; Kim, C.; Khil, M.; Park, S. *Nanotechnology* **2003**, *14*, 532−537. (b) Li, D.; Xia, Y. N. *Nano Lett.* **2003**, *3*, 555−560. (c) Madhugiri, S.; Sun, B.; Smirniotis, P. G.; Ferraris, J. P.; Balkus, K. J. *Microporous Mesoporous Mater.* **2004**, *69*, 77−83. (d) Onozuka, K.; Ding, B.; Tsuge, Y.; Naka, T.; Yamazaki, M.; Sugi, S.; Ohno, S.; Yoshikawa, M.; Shiratori, S. *Nanotechnology* **2006**, *17*, 1026−1031.

(9) (a) Farmer, D. B.; Gordon, R. G. *J. Appl. Phys.* **2007**, 101. (b) Hsu, I. J.; Hansgen, D. A.; McCandless, B. E.; Willis, B. G.; Chen, J. G. *J. Phys. Chem. C* **2011**, *115*, 3709−3715. (c) Christensen, S. T.; Elam, J. W.; Rabuffetti, F. A.; Ma, Q.; Weigand, S. J.; Lee, B.; Seifert, S.; Stair, P. C.; Poeppelmeier, K. R.; Hersam, M. C.; Bedzyk, M. J. *Small* **2009**, *5*, 750−757. (d) Park, H.; Kim, A.; Lee, C.; Lee, J. S.; Lee, J. *Appl. Phys. Lett.* **2009**, 94.

(10) (a) Choi, J.; Park, H.; Hoffmann, M. R. *J. Phys. Chem. C* **2010**, *114*, 783−792. (b) Klosek, S.; Raftery, D. *J. Phys. Chem. B* **2001**, *105*, 2815−2819.

(11) Archana, P. S.; Jose, R.; Jin, T. M.; Vijila, C.; Yusoff, M. M.; Ramakrishna, S. *J. Am. Ceram. Soc.* **2010**, *93*, 4096−4102.

(12) (a) Liu, J.; Yang, H. T.; Tan, W. W.; Zhou, X. W.; Lin, Y. A. *Electrochim. Acta* **2010**, *56*, 396−400. (b) Niishiro, R.; Kato, H.; Kudo, A. *Phys. Chem. Chem. Phys.* **2005**, *7*, 2241−2245.

(13) Sheppard, L. R.; Bak, T.; Nowotny, J.; Nowotny, M. K. *Int. J. Hydrogen Energy* **2007**, *32*, 2660−2663.

(14) (a) Arbiol, J.; Cerda, J.; Dezanneau, G.; Cirera, A.; Peiro, F.; Cornet, A.; Morante, J. R. *J. Appl. Phys.* **2002**, *92*, 853−861. (b) Bernasik, A.; Radecka, M.; Rekas, M.; Sloma, M. *Appl. Surf. Sci.* **1993**, *65*−*6*, 240−245.

(15) Paredis, K.; Ono, L. K.; Mostafa, S.; Li, L.; Zhang, Z. F.; Yang, J. C.; Barrio, L.; Frenkel, A. I.; Cuenya, B. R. *J. Am. Chem. Soc.* **2011**, *133*, 6728−6735.

(16) Feng, Z. X.; Christensen, S. T.; Elam, J. W.; Lee, B.; Hersam, M. C.; Bedzyk, M. J. *J. Appl. Phys.* **2011**, 110.

(17) (a) Dameron, A. A.; Pylypenko, S.; Bult, J. B.; Neyerlin, K. C.; Engtrakul, C.; Bochert, C.; Leong, G. J.; Frisco, S. L.; Simpson, L.; Dinh, H. N.; Pivovar, B. *Appl. Surf. Sci.* **2012**, *258*, 5212−5221. (b) Liu, C.; Wang, C. C.; Kei, C. C.; Hsueh, Y. C.; Perng, T. P. *Small* **2009**, *5*, 1535−1538.

(18) (a) de Miguel, S. R.; Scelza, O. A.; Roman-Martinez, M. C.; de Lecea, C. S. M.; Cazorla-Amoros, D.; Linares-Solano, A. *Appl. Catal., A* **1998**, *170*, 93−103. (b) Suh, D. J.; Park, T. J.; Ihm, S. K. *Carbon* **1993**, *31*, 427−435. (c) Torres, G. C.; Jablonski, E. L.; Baronetti, G. T.; Castro, A. A.; de Miguel, S. R.; Scelza, O. A.; Blanco, M. D.; Jimenez, M. A. P.; Fierro, J. L. G. *Appl. Catal., A* **1997**, *161*, 213−226.

(19) (a) Gu, D. F.; Baumgart, H.; Tapily, K.; Shrestha, P.; Namkoong, G.; Ao, X. Y.; Muller, F. *Nano Res.* **2011**, *4*, 164−170. (b) Setthapun, W.; Williams, W. D.; Kim, S. M.; Feng, H.; Elam, J. W.; Rabuffetti, F. A.; Poeppelmeier, K. R.; Stair, P. C.; Stach, E. A.; Ribeiro, F. H.; Miller, J. T.; Marshall, C. L. *J. Phys. Chem. C* **2010**, *114*, 9758−9771.

(20) (a) Huang, Z. C.; Feng, J.; Pan, W. *Rare Metal Mater. Eng.* **2011**, *40*, 475−477. (b) Liu, X. D.; Jiang, E. Y.; Li, Z. Q.; Song, Q. G. *Appl. Phys. Lett.* **2008**, *92*, 1−3.

(21) Tasaki, C.; Oka, N.; Yagi, T.; Taketoshi, N.; Baba, T.; Kamiyama, T.; Nakamura, S.; Shigesato, Y. *Jpn. J. Appl. Phys.* **2012**, 51.

(22) (a) Jung, S. Y.; Ha, T. J.; Seo, W. S.; Lim, Y. S.; Shin, S.; Cho, H. H.; Park, H. H. *J. Electron. Mater.* **2011**, *40*, 652−656. (b) Nguyen, S. T.; Yang, Y. H.; Wang, X. *Appl. Catal., B* **2012**, *113*, 261−270.

(23) (a) Bezerra, C. W. B.; Zhang, L.; Liu, H. S.; Lee, K. C.; Marques, A. L. B.; Marques, E. P.; Wang, H. J.; Zhang, J. J. *J. Power Sources* **2007**, *173*, 891−908. (b) Antolini, E.; Cardellini, F.; Giacometti, E.; Squadrito, G. *J. Mater. Sci.* **2002**, *37*, 133−139. (c) Han, K. S.; Moon, Y. S.; Han, O. H.; Hwang, K. J.; Kim, I.; Kim, H. *Electrochem. Commun.* **2007**, *9*, 317−324.

(24) Pan, H.; Zhang, Y. W.; Shenoy, V. B.; Gao, H. J. *J. Phys. Chem. C* **2011**, *115*, 12224−12231.